(Received 5 May 2024, Accepted 10 July 2024, Scheduled 18 July 2024)

Canay Inductance Impact Characterization on Dynamic Behaviour of Synchronous Machines

Farid Leguebedj[1]*, Djamel Boukhetala[2], and Madjid Teguar[1]

[1]*Laboratoire de Recherche en Electrotechnique (LRE), Ecole Nationale Polytechnique 10 Rue des frères OUDEK, El-Harrach, 16200, Algiers, Algeria*
[2]*Laboratoire de Commande des Processus (LCP), Ecole Nationale Polytechnique 10 Rue des frères OUDEK, El-Harrach, 16200, Algiers, Algeria*

ABSTRACT: The conventional synchronous generator model accurately represents only the stator circuit. However, when considering transient effects on rotor quantities such as rotor voltage and current, accurate predictions can be achieved by properly incorporating the field and damper considerations with the stator circuits in an equivalent model. Besides, it has been observed that simulated responses obtained using the conventional model with calculated machine parameters frequently do not align well with the actual measured responses, especially for the rotor winding. This paper analyzes the effect of the d and q axis parameters of synchronous machines, focusing on accurately determining these parameters, particularly the Canay inductance. It investigates the impact of precise determination of these parameters from the time constants of the direct axis operational inductance on transient response and stability. Through simulation studies on a high order model synchronous generator system, the paper compares transient performances with and without considering Canay inductance, shedding light on its effects.

List of Symbols

L_c: Canay inductance
X_c: Canay reactance
X_{rc}: Characteristic rotor reactance
s: Laplace's operator
ω_s, ω_B: Synchronous speed, basic angular frequency
V_d, V_q: d-axis stator voltage, q-axis stator voltage
i_d, i_q, i_f: d-axis current, q-axis current, and field current
i_{kd1}, i_{kd2}: d-axis dampers currents
i_{kq1}, i_{kq2}, i_{kq3}: q-axis dampers currents
V_f: d-axis field voltage
$L_d(s)$: d-axis operational inductance
$L_q(s)$: q-axis operational inductance
L_d, L_q, L_f: d-axis synchronous inductance, q-axis synchronous inductance, field inductance
X_d, X_q: d-axis synchronous reactance, q-axis synchronous reactance
R_a, R_f: armature and field resistances
R_k, R_j: d-axis damper resistances
R_{kq1}, R_{kq2}, R_{kq3}: q-axis damper resistances
L_k, L_J: d-axis damper inductances
L_{kq1}, L_{kq2}, L_{kq3}: q-axis damper inductances
L_{md}: d-axis magnetizing inductance
L_{mq}: q-axis magnetizing inductance
L_a: leakage inductance
X_a: leakage reactance
L_{amd}: the parallel combination of L_{md} and L_a
T'_{d0}, T'_d: d-axis transient open circuit and short-circuit time constant
T'_{q0}, T'_q: q-axis transient open circuit and short-circuit time constant
T''_{d0}, T''_d: d-axis sub-transient open circuit and short-circuit time constant
T''_{q0}, T''_q: q-axis sub-transient open circuit and short-circuit time constant
T'''_{d0}, T'''_d: d-axis sub-subtransient open circuit and short-circuit time constant
T'''_{q0}, T'''_q: d-axis sub-sub-transient open circuit and short-circuit time constant
$\dot{\omega}$: rotor angular speed in pu
δ: load angle in degrees

1. INTRODUCTION

Synchronous generators have a great influence on the stability of power systems, and improving the accuracy of their models is extremely important in analyzing the dynamic characteristics of power systems. Park's d- and q-axis models are generally the most commonly used synchronous machine models for system modeling [1–4]. Various other models can be effectively applied in power system stability studies [5–8].

In reviewing such research, the standard model for studying the transient responses of the synchronous machine is the second order model. It is very useful for studying dynamic stability but is not suitable for considering generator performance regarding control experiments, which creates different results with measurements [9–12].

* Corresponding author: Farid Leguebedj (farid.leguebedj@g.enp.edu.dz).

The conventional stability theory of generator models relies on the assumption that the mutual inductances among the armature, dampers, and field windings on the direct axis are similar. This hypothesis forms the foundation for analyzing the stability of generators [13–15]. Additionally, the damper windings positioned close to the air-gap induce flux that closely interacts with the armature flux. This assumption has proven effective in yielding favorable results for stability analysis, especially those concerning the network side [16–18].

However, when delving into the investigation of field current behavior, a significant discrepancy arises. In transient responses, field current measurements have revealed substantially higher alternating amplitudes [13]. The conventional two-axis framework model primarily focuses on the armature circuit, neglecting the additional inductance that signifies the difference between the reciprocated inductances of the field-damper and field-armature circuits on the d-axis. Incorporating this additional inductance into the model is necessary for accuracy [14].

The Canay inductance, denoted by X_c, plays a crucial role in influencing the leakage flux, and is identified by test or by geometry [15]. If we overlook the Canay inductance, both the base current of the field winding and armature leakage inductance are considered independent variables [13–15, 19]. The extent of leakage inductance might differ from the value specified by the real machine [18].

A structured method was introduced to identify substitute circuits that replicate the frequency behavior of magnetic component input impedance across a wide range of frequencies [20].

An alternative method involves modeling it alongside the conventional perspective on how current paths are divided within the physical structure [21, 22].

This study presents a method for analyzing the stability of synchronous generators by considering different mutual inductances among armature, dampers, and field windings on the direct axis. It outlines the process of creating an equivalent model and highlights the benefits of this model compared to traditional ones. Section 2 introduces the Canay model. Section 3 provides a detailed mathematical analysis of the 3^{rd} order model. Section 4 discusses the modeling of the synchronous machine. Section 5 describes the methodology. Section 6 focuses on studying the impact of Canay inductance on the dynamic behavior of the machine. Concluding remarks are presented in the last section.

2. HIGHER ORDER MODEL OF SYNCHRONOUS MACHINE (CANAY MODEL)

The armature, field, and damper windings of a synchronous machine are magnetically coupled not only in the main field, but also in the dispersion field.

Starting from the fundamental equations of the idealized synchronous machine [13–15] and taking into account the real magnetic coupling between the damping field windings, we can deduce the equivalent diagram of Figure 1.

The characteristic rotor reactance X_{rc} appears on the current path common to the damping and field circuits, and it is obtained using the following well-known equation, [13–15]:

$$\frac{1}{X_{rc}} + \frac{1}{X_d - X_a} = \frac{1}{X_c - X} \tag{1}$$

X_c represents the Canay reactance, and X_a is the leakage reactance.

The proof of Equation (1) is given in Appendix A.

We recall that:

$$X_c = \omega_s L_c, \quad X_{rc} = \omega_s L_{rc} \tag{2}$$

Taking $X = X_c$ and according to the previous equation, we get $X_{rc} = 0$. In practice, we take $X = X_a$, thus the leakage reactance of the armature, which does not include the rotor circuits, is considered as an external reactance, which is justified. However, in this choice the reactance X_{rc} does not cancel out.

This is the main difference between the new and classic equivalent schemes. It can be concluded that, for an exact representation of rotor circuits, it is necessary to introduce the reactances X_c and X_{rc} [13–15].

The diagram in Figure 1 is equivalent to the diagram in Figure 3 [13, 25, 26].

3. ANALYSIS OF THE 3rd ORDER MODEL OF THE SYNCHRONOUS MACHINE

This section aims to present the expression of the operational inductance $L_d(s)$ and $L_q(s)$ as function of (i) the equivalent circuit parameters, and (ii) the time constants and synchronous inductance.

For this purpose, we have used the conventional third-order equivalent circuit model, depicted in Figure 1, with ($L_c = L_a$). Lacking the rotor leakage reactance this circuit is relatively simple. The symbols X_a and X_{md} denote the armature leakage reactance and armature magnetizing reactance. The combination of R_f and L_f represents the short-circuited field winding Z_f. Furthermore, R_k and L_k symbolize the damper windings Z_k, while R_j and L_j incorporate the rotor eddy currents Z_J.

Initially, the consolidation process merged the four parallel branches into a unified impedance designated as Z'.

$$Z'(s) = sL_{md}//Z_f//Z_k//Z_J \tag{3a}$$

$$= \frac{sL_{md}Z_fZ_kZ_J}{sL_{md}Z_fZ_k + sL_{md}Z_fZ_J + sL_{md}Z_kZ_J + Z_fZ_kZ_J} \tag{3b}$$

As mentioned earlier,

$$sL_d(s) = Z'(s) + sL_a \tag{4a}$$

The relationship is depicted in Figure 1. It illustrates the parallel combination previously described, now connected in series with the armature leakage reactance sL_a, for the conventional model.

$$L_d(s) = \frac{sL_aZ_fZ_kZ_J + s^2L_aZ_fZ_kL_{md} + s^2L_aZ_fZ_jL_{md} + s^2L_aZ_kZ_jL_{md} + sL_{md}X_fZ_jZ_k}{sL_{md}Z_fZ_k + sL_{md}Z_fZ_J + sL_{md}Z_kZ_J + Z_fZ_kZ_J} \tag{4b}$$

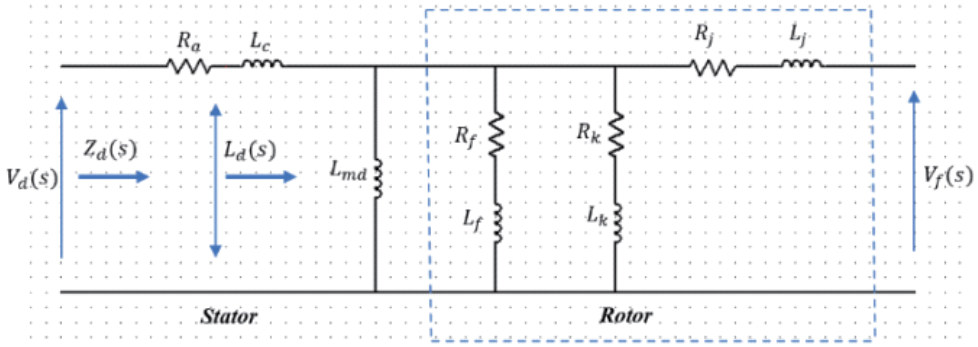

FIGURE 1. Equivalent circuit of a third order model for direct axis (with canay inductance L_c).

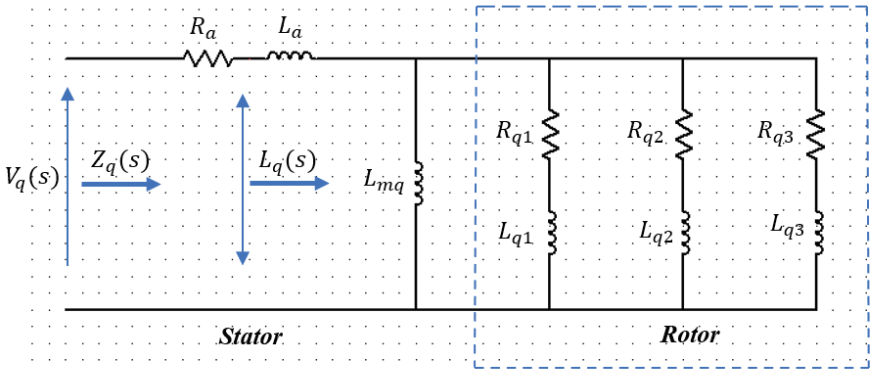

FIGURE 2. Equivalent circuit of a third order model for quadrature axis.

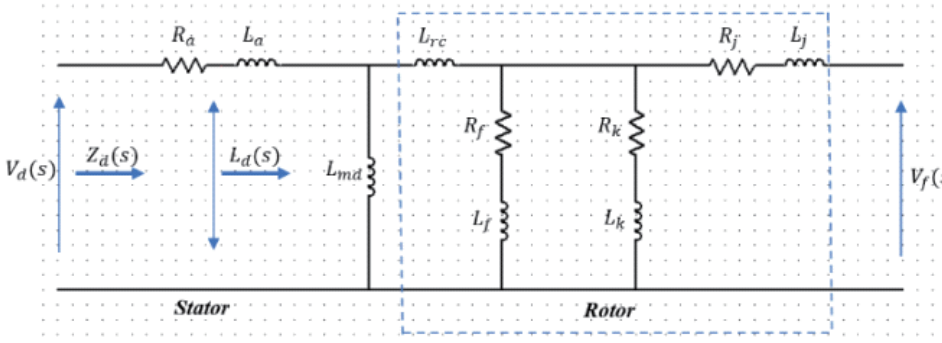

FIGURE 3. Equivalent Circuit of a third order model for direct axis (with L_{rc} inductance).

In order to facilitate the analysis, we proceeded to examine the numerator and denominator separately. Our initial focus was on the numerator. We replaced Z_f, Z_k, and Z_J with their actual terms in the numerator. The new expressions are shown below.

$$Z_f = R_f + sL_f, \quad Z_k = R_k + sL_k, \quad Z_j = R_j + sL_j \tag{5}$$

The symbol "Num" is used to represent the numerator. It is presented in the following manner:

$$\begin{aligned} Num &= sL_a(R_f+sL_f)(R_k+sL_k)(R_j+sL_j) \\ &+sL_a(R_f+sL_f)(R_k+sL_k)sL_{md} \\ &+sL_a(R_f+sL_f)(R_j+sL_j)sL_{md}+sL_a(R_k+sL_k) \\ &(R_j+sL_j)sL_{md}+(R_f+sL_f)(R_k+sL_k)(R_j+sL_j)sL_{md} \end{aligned} \tag{6a}$$

By simplifying the previous expression, we obtain:

$$\begin{aligned} Num &= s(L_aR_fR_kR_j)+s^2[L_aL_{md}(R_fR_k+R_fR_j+R_jR_k) \\ &+L_a(R_fR_kL_j+R_fR_jR_k+R_kR_jL_f) \\ &+L_{md}(R_fR_kL_j+R_fR_jR_k+R_kR_jL_f)] \\ &+s^3[L_a(R_fL_kL_J+R_fL_JR_k+R_kL_fL_j) \\ &+L_aL_{md}(R_fL_k+R_fL_j+R_kL_f+R_kL_j+R_jL_f+R_jL_k) \\ &+L_{md}(R_fL_kL_j+R_kL_fL_j+R_jL_fL_k)] \\ &+s^4(L_aL_fL_kL_j+L_fL_kL_j) \end{aligned} \tag{6b}$$

Using $L_{amd} = \frac{L_a L_{md}}{L_a + L_{md}}$, inserting this expression into the numerator, and factoring out the term $s(L_a + L_{md})$, then dividing the equation by $R_f R_k R_j$, we get the following expression:

$$Num = \frac{(La+L_{md})}{R_f R_k R_j}\left[1+s\left(\frac{L_f+L_{amd}}{Rf}+\frac{L_k+L_{amd}}{R_k}\right.\right.$$
$$\left.+\frac{L_j+L_{amd}}{R_j}\right)+s^2\left(\frac{L_{amd}L_f+L_{amd}L_k+L_fL_k}{RfRk}\right.$$
$$\left.+\frac{L_{amd}L_f+L_{amd}L_j+L_fL_j}{R_fR_j}+\frac{L_{amd}L_k+L_{amd}L_j+L_kL_j}{R_kR_j}\right)$$
$$\left.+s^3\left(\frac{L_fL_kL_j+L_{amd}L_fL_k+L_{amd}L_fL_j+L_{amd}L_kL_j}{R_fR_kR_j}\right)\right] \quad (6c)$$

The denominator "Den" follows the same structure of the numerator, except that L_{amd} is replaced by L_{md}.

$$Den = \frac{1}{R_f R_k R_j}[1+s\left(\frac{L_f+L_{md}}{Rf}+\frac{L_k+L_{md}}{R_k}+\frac{L_j+L_{md}}{R_j}\right)$$
$$+s^2\left(\frac{L_{md}L_f+L_{md}L_k+L_fL_k}{RfRk}+\frac{L_{md}L_f+L_{amd}L_j+L_fL_j}{R_fR_j}\right.$$
$$\left.+\frac{L_{md}L_k+L_{md}L_j+L_kL_j}{R_kR_j}\right)$$
$$+s^3\left(\frac{L_fL_kL_j+L_{md}L_fL_k+L_{md}L_fL_j+L_{md}L_kL_j}{R_fR_kR_j}\right) \quad (7a)$$

So,

$$L_d(s) = \frac{Num}{Den} \quad (7b)$$

The operational inductance for a third-order model can be expressed as follows:

$$L_d(s) = L_d\frac{(1+sT'_d)(1+sT''_d)(1+sT'''_d)}{(1+sT'_{d0})(1+sT''_{d0})(1+sTT'''_{d0})} \quad (8)$$

Figure 2 shows the equivalent circuit of the 3rd order model along the q-axis. Equation (8) remains applicable to the q-axis as well:

$$L_q(s) = L_q\frac{(1+sT'_q)(1+sT''_q)(1+sT'''_q)}{(1+sT'_{q0})(1+sT''_{q0})(1+sT'''_{q0})} \quad (9)$$

When using the Canay model, we replace leakage inductance L_a by L_c (Canay inductance).

The development of $L_d(s)$ in terms of equivalent circuit parameters and in terms of time constants and synchronous inductance allows obtaining the nonlinear system of equations presented in Subsection 5.1. As inputs to our system, we have used the time constants cited in [24]. The outputs are the equivalent circuit parameters. Such parameters are introduced in Equation (7b) to calculate the operational inductance $L_d(s)$. In order to validate our calculation, the frequency response of this operational inductance will be compared to that given by Equation (8).

The operational inductance $L_q(s)$ is determined by the same mathematical procedure replacing d by q in previous expressions.

4. SYNCHRONOUS MACHINE MODELING

The aim of this section is to develop the model of the synchronous machine. This model is constituted by differential equations where the state variables are the flux, and the coefficients are the parameters of the equivalent circuits according to the d-axis and q-axis cited in Sections 2 and 3.

The traditional representation of the synchronous machine involves three stator windings, a field winding, a d-axis damper winding, and two q-axis damper windings [1, 2]. A variable transformation process allows obtaining a set of voltage equations for each winding that remains the same even regardless of the movement of the rotor. This transformation entails the change of the stator reference frame abc into a rotor reference frame $qd0$, which is accomplished through the application of Park's Transformation [1, 2].

$$P = \frac{2}{3}\begin{bmatrix} \cos(\vartheta) & \cos(\vartheta-\frac{2\pi}{3}) & \cos(\vartheta+\frac{2\pi}{3}) \\ \sin(\vartheta) & \sin(\vartheta-\frac{2\pi}{3}) & \sin(\vartheta+\frac{2\pi}{3}) \\ \frac{1}{2} & \frac{1}{2} & \frac{1}{2} \end{bmatrix} \quad (10)$$

The value of the angle ϑ is determined by:

$$\vartheta = \omega_s t + \delta - \frac{\pi}{2} \quad (11)$$

In Equation (11), ω_s represents the electrical angular speed at synchronous conditions in radians per second, and δ signifies the power angle in electrical radians.

The equations describing voltage in the $qd0$ reference frame are as follows:

$$V_{qd0s} = -R_{sn}i_{qd0s} + \omega\psi_{dqs} + \dot{\psi}_{qd0s} \quad (12)$$

$$V_{qdr} = R_r i_{qdr} + \dot{\psi}_{qdr} \quad (13)$$

Here,

$$V_{qd0s} = [v_q v_d v_0]^T, \quad R_{sn} = diag[r_s r_s r_s],$$
$$\psi_{qd0s} = [\psi_q \psi_d \psi_0]^T, \quad I_{qds} = [i_q i_d]^T \quad (14)$$

ω is the rotor speed in per-unit.

Similarly, the rotor equations in (13) involve:

$$\begin{aligned} V_{qdr} &= [v_{kq1} v_{kq2} v_f v_{kd1}]^T, \\ R_r &= \text{diag}[r_{kq1} r_{kq2} r_f r_{kd1}], \\ \psi_{qdr} &= [\psi_{kq1} \psi_{kq2} \psi_f \psi_{kd1}]^T, \\ I_{qdr} &= [i_{kq1} i_{kq2} i_f i_{kd1}]^T \end{aligned} \quad (15)$$

Selecting the appropriate rotor base quantities allows expressing the relationship between flux and current using magnetizing reactances (X_{md} and X_{mq}) and the leakage reactance for each winding (X_a, X_{kq1}, X_{kq2}, X_f, and X_{kd1}).

$$\begin{aligned} X_d &= X_a + X_{md}, & X_q &= X_a + X_{mq}, \\ X_F &= X_f + X_{md}, & X_{Q1} &= X_{kq1} + X_{mq} \\ X_{KD1} &= X_{kd1} + X_{md}, & X_{Q2} &= X_{kq2} + X_{mq} \end{aligned} \quad (16)$$

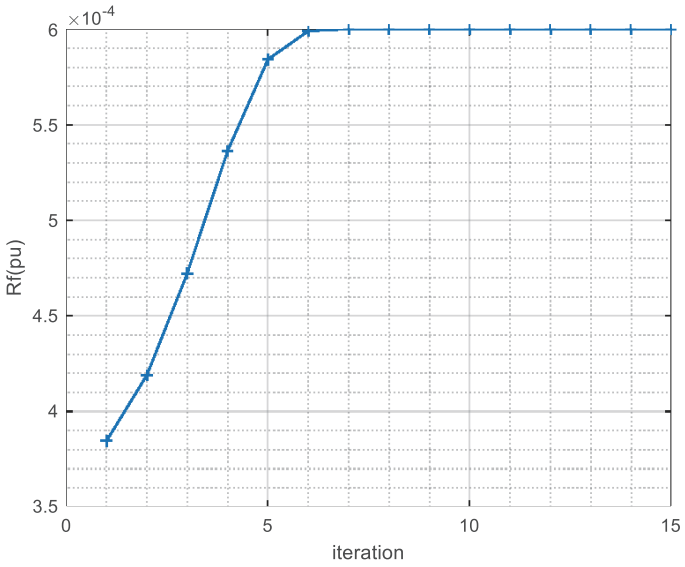

FIGURE 4. Variation of inductance R_f versus Iteration (with X_c).

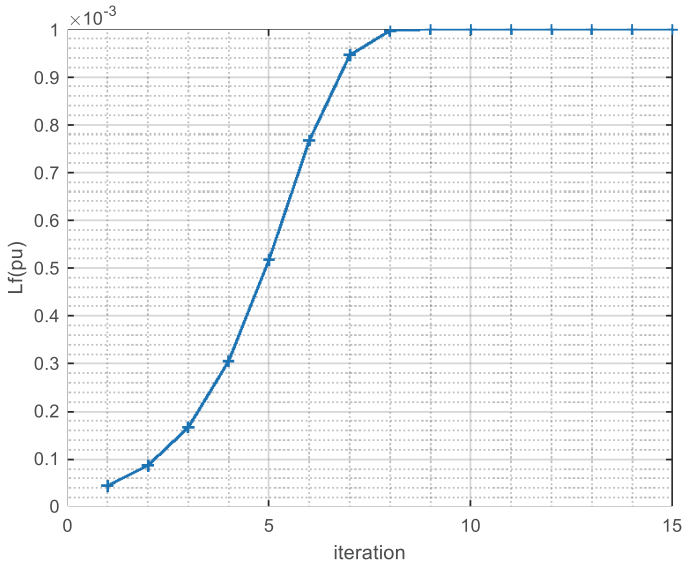

FIGURE 5. Variation of inductance L_f versus Iteration (with X_c).

$$\begin{bmatrix} \psi_q \\ \psi_d \\ \psi_{kq1} \\ \psi_{kq2} \\ \psi_f \\ \psi_{kd1} \end{bmatrix} = \begin{bmatrix} -X_q & 0 & 0 & X_{mq} & X_{mq} & 0 & 0 \\ 0 & -X_d & 0 & 0 & 0 & X_{md} & X_{md} \\ -X_{mq} & 0 & 0 & X_{Q1} & X_{mq} & 0 & 0 \\ -X_{mq} & 0 & 0 & X_{mq} & X_{Q2} & 0 & 0 \\ 0 & -X_{md} & 0 & 0 & 0 & X_F & X_{md} \\ 0 & -X_{md} & 0 & 0 & 0 & X_{md} & X_{KD1} \end{bmatrix} \begin{bmatrix} i_q \\ i_d \\ i_{kq1} \\ i_{kq2} \\ i_f \\ i_{kd1} \end{bmatrix} \tag{17}$$

The solutions for Equations (12) and (13) can be found using Equation (17), as described in [27].

$$\dot{\psi_q} = \omega_B \left(v_q - \dot{\omega}\dot{\psi_d} + \frac{r_s}{X_l} \left(\dot{\psi_{mq}} - \dot{\psi_q} \right) \right) \tag{18}$$

$$\dot{\psi_d} = \omega_B \left(v_d - \dot{\omega}\dot{\psi_q} + \frac{r_s}{X_a} \left(\dot{\psi_{md}} - \dot{\psi_d} \right) \right) \tag{19}$$

$$\dot{\psi}_{kq11} = \omega_B \left(v_{kq1} + \frac{r_{kq1}}{X_{kq1}} \left(\dot{\psi_{mq}} - \dot{\psi_{kq1}} \right) \right) \tag{20}$$

$$\dot{\psi_{kq2}} = \omega_B \left(v_{kq2} + \frac{r_{kq2}}{X_{kq2}} \left(\dot{\psi_{mq}} - \dot{\psi_{kq2}} \right) \right) \tag{21}$$

$$\dot{\psi_f} = \omega_B \left(v_f + \frac{r_f}{X_f} \left(\dot{\psi_{md}} - \dot{\psi_f} \right) \right) \tag{22}$$

$$\dot{\psi}_{kd1} = \omega_B \left(v_{kd1} + \frac{r_{kd1}}{X_{kd1}} \left(\dot{\psi_{md}} - \dot{\psi_{kd1}} \right) \right) \tag{23}$$

$$\dot{\psi_{mq}} = X_{aq} \left(\frac{\dot{\psi_q}}{X_a} + \frac{\dot{\psi_{kq1}}}{X_{kq1}} + \frac{\dot{\psi_{Kq2}}}{X_{kq2}} \right) \tag{24}$$

$$\dot{\psi_{md}} = X_{ad} \left(\frac{\dot{\psi_d}}{X_a} + \frac{\dot{\psi_f}}{X_f} + \frac{\dot{\psi_{kd1}}}{X_{kd1}} \right) \tag{25}$$

$$X_{aq} = \left(\frac{1}{X_{mq}} + \frac{1}{X_a} + \frac{1}{X_{kq1}} + \frac{1}{X_{kq2}} \right)^{-1} \tag{26}$$

$$X_{ad} = \left(\frac{1}{X_{md}} + \frac{1}{X_a} + \frac{1}{X_f} + \frac{1}{X_{kd1}} \right)^{-1} \tag{27}$$

where ω_B denotes the basic angular frequency in radians per second, with all other variables expressed in per-unit. The differential equations describing the rotor dynamics are as follow:

$$\dot{\omega} = \frac{1}{2H}(T_u - T_e) \tag{28}$$

$$\dot{\delta} = \omega_B \dot{\omega} - \omega_s \tag{29}$$

H represents the machine inertia constant measured in seconds. T_u stands for mechanical torque, while T_e refers to electrical torque, both expressed in per unit (pu). The electrical torque, denoted as T_e, is defined by the following expression:

$$T_e = \dot{\psi_d} i_q - \dot{\psi_q} i_d \tag{30}$$

The fluxes provide a convenient method for illustrating the currents, as stated in [27]

$$i_q = \frac{1}{X_a}(\dot{\psi_{mq}} - \dot{\psi_q}) \tag{31}$$

$$i_d = \frac{1}{X_a}(\dot{\psi_{md}} - \dot{\psi_d}) \tag{32}$$

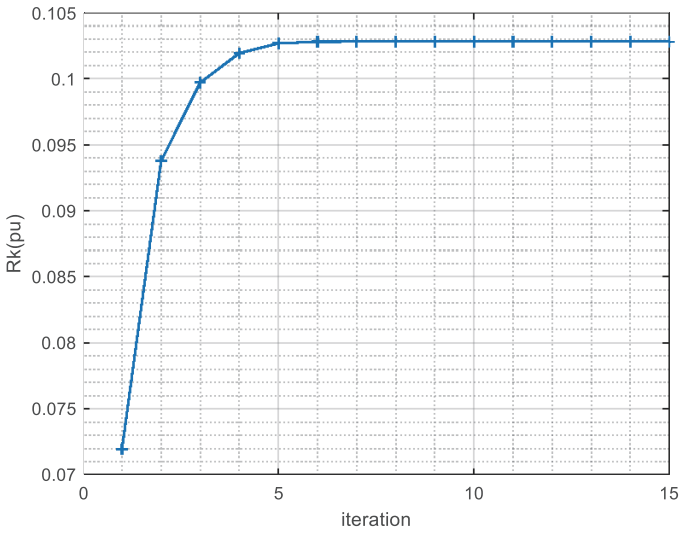

FIGURE 6. Variation of inductance R_k versus Iteration (with X_c).

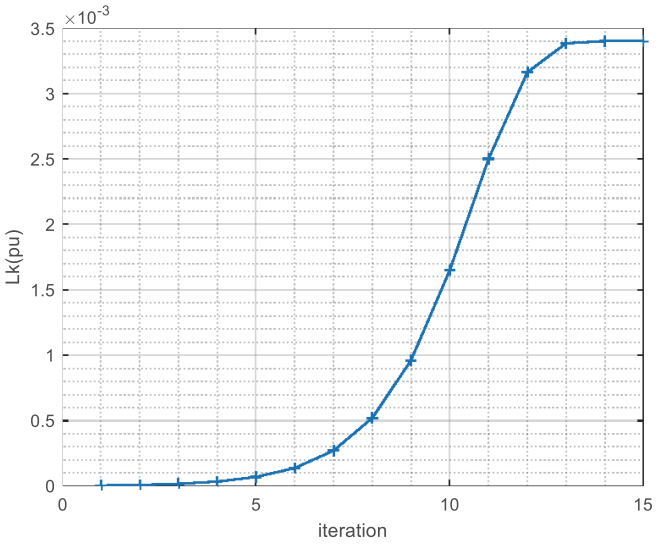

FIGURE 7. Variation of inductance L_k versus Iteration (with X_c).

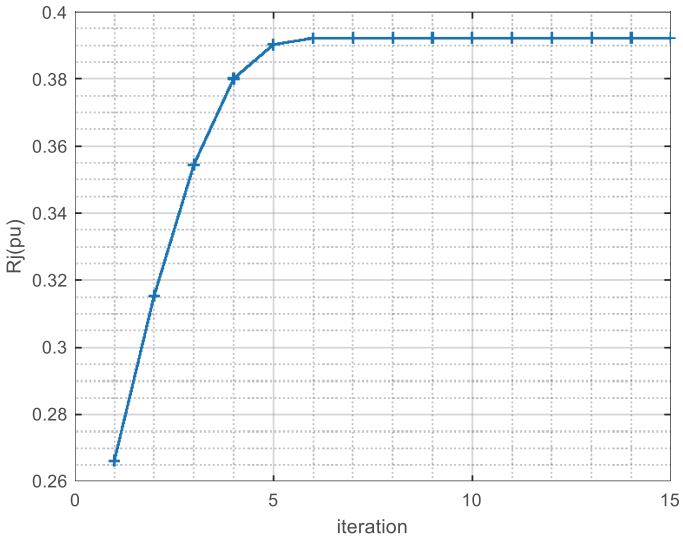

FIGURE 8. Variation of inductance R_f versus Iteration (with X_c).

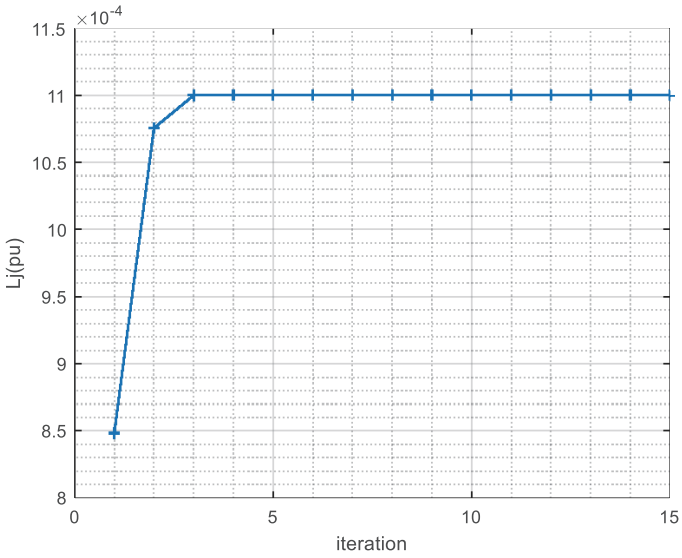

FIGURE 9. Variation of inductance L_j versus Iteration (with X_c).

$$i_f = \frac{1}{X_f}(\dot{\psi_f} - \dot{\psi_{md}}) \tag{33}$$

The currents flowing through the dampers winding can also be expressed by:

$$i_{kd1} = \frac{1}{X_{kd1}}(\dot{\psi_{kd1}} - \dot{\psi_{md}}) \tag{34}$$

$$i_{kq1} = \frac{1}{X_{kq1}}(\dot{\psi_{kq1}} - \dot{\psi_{mq}}) \tag{35}$$

$$i_{kq2} = \frac{1}{X_{kq2}}(\dot{\psi_{kq2}} - \dot{\psi_{mq}}) \tag{36}$$

5. METHODOLOGY

This study outlines a design approach comprising two principal segments. The initial phase deals with the definition of the parameters of the d-axis equivalent circuits for the third model, with and without Canay reactance X_c, as well as the q-axis parameters. The second phase investigates how the characteristic reactance X_c influences the dynamic characteristics of the machine.

5.1. D-Axis and q-Axis Parameter

The characteristics of the rotor network are determined by solving a group of equations simultaneously. These equations utilize the standard impedances and time constants of the generator. Refs. [5, 23] outline these equations, which are used to identify the parameters of the rotor network from time constants.

All values of circuit equivalent parameters and inductances are in per-unit, and ω_s represents the synchronous speed of the machine in electrical radians per second.

TABLE 1. Third order model characteristic quantities.

$X_d = 1.59\,\text{pu}$	$X'_d = 0.317\,\text{pu}$	$X''_d = 0.264\,\text{pu}$	$X'''_d = 0.186\,\text{pu}$
$X_c = 0.0546\,\text{pu}$	$T'_d = 2.12\,\text{s}$	$T''_d = 0.0343\,\text{s}$	$T'''_d = 0.0032\,\text{s}$
$X_{rc} = -0.071\,\text{pu}$	$T'_{d0} = 10.7\,\text{s}$	$T''_{d0} = 0.0413\,\text{s}$	$T'''_{d0} = 0.0045\,\text{s}$
$X_q = 1.08\,\text{pu}$	$X'_q = 0.71\,\text{pu}$	$X''_q = 0.334\,\text{pu}$	$X'''_q = 0.167\,\text{pu}$
	$T'_q = 0.285\,\text{s}$	$T''_q = 0.0221\,\text{s}$	$T'''_q = 0.0032\,\text{s}$
	$T'_{q0} = 0.453\,\text{s}$	$T''_{q0} = 0.0491\,\text{s}$	$T'''_{q0} = 0.0058\,\text{s}$

TABLE 2. Estimation of equivalent circuit parameters.

Parameters	with X_c	without X_c
L_f (pu)	0.0010	0.0007
R_f (pu)	0.0006	0.0005
L_k (pu)	0.0034	0.0017
R_k (pu)	0.1028	0.0557
L_j (pu)	0.0011	0.0003
R_j (pu)	0.3932	0.1619
L_{q1} (pu)	0.005	0.005
R_{q1} (pu)	0.0188	0.0188
L_{q2} (pu)	0.0013	0.0013
R_{q2} (pu)	0.0758	0.0758
L_{q3} (pu)	0.0002	0.0002
R_{q3} (pu)	0.1270	0.1270

The third-order model is represented by the following system of equations.

$$L_{md} = L_d - L_a \tag{37}$$

$$T'_{d0} = \frac{1}{Rf}(Lf + L_{md}) \tag{38}$$

$$T'_d = \frac{1}{Rf}\left(Lf + \frac{L_{md}L_a}{L_{md}+L_a}\right) \tag{39}$$

$$T''_{d0} = \frac{1}{Rk}\left(Lk + \frac{L_{md}L_f}{L_{md}+L_f}\right) \tag{40}$$

$$T''_d = \frac{1}{Rk}\left(Lk + \frac{L_{md}L_aL_f}{L_{md}L_a + L_{md}L_f + L_aL_f}\right) \tag{41}$$

$$T'''_{d0} = \frac{1}{Rj}\left(Lj + \frac{L_{md}L_fL_k}{L_{md}L_f + L_{md}L_k + L_fL_k}\right) \tag{42}$$

$$T'''_d = \frac{1}{Rj}\left(Lj + \frac{L_{md}L_aL_fL_k}{L_{md}L_aL_f + L_{md}L_aL_k + L_{md}L_fL_k + L_aL_fL_k}\right) \tag{43}$$

By replacing d by q, the previous system of nonlinear equations can be used for the q-axis. The system inputs are the q-axis time constants cited in [24], while the outputs are the parameters of the equivalent circuit.

5.2. Estimation of Equivalent Circuit Parameters

In order to apply our approach, we utilized data from [24]. These data consider a salient-pole machine with solid poles, characterizing by a power of $S_n = 230\,\text{MVA}$, stator resistance $R_a = 0.005\,\text{pu}$, leakage inductance $L_a = 0.00041\,\text{pu}$, power factor $\cos(\varphi) = 0.85$, mechanical time constant $H = 3.8\,\text{s}$, and Canay inductance $X_c = 0.0546\,\text{pu}$.

For the rotor circuit, the data for the 3^{rd} order model are the time constants, the synchronous reactances along the d axis and q axis, and the characteristic rotor reactance, cited in Table 1.

The nonlinear equations presented in Subsection 5.1 were subjected to simulation via the Newton-Raphson method in MATLAB. The time constants were designated as inputs, while the equivalent circuit parameters were designated as outputs.

We get the Canay model when replacing the leakage inductance L_a by the L_c (Canay inductance).

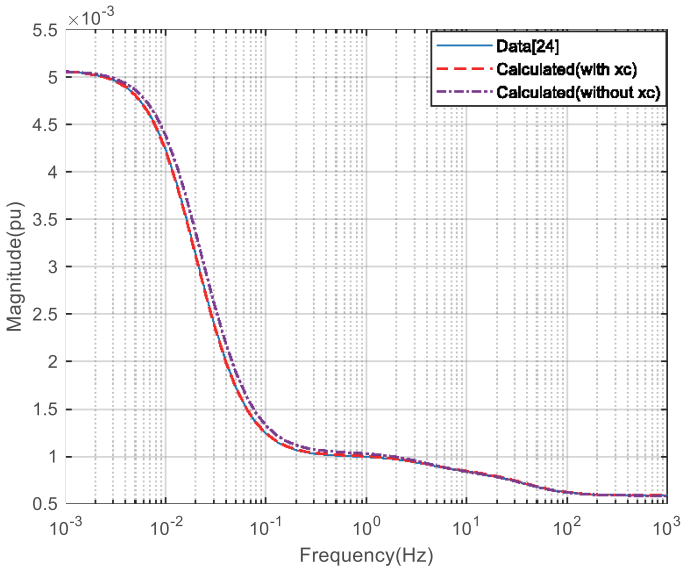

FIGURE 10. Operational inductance magnitude versus frequency (d-axis)

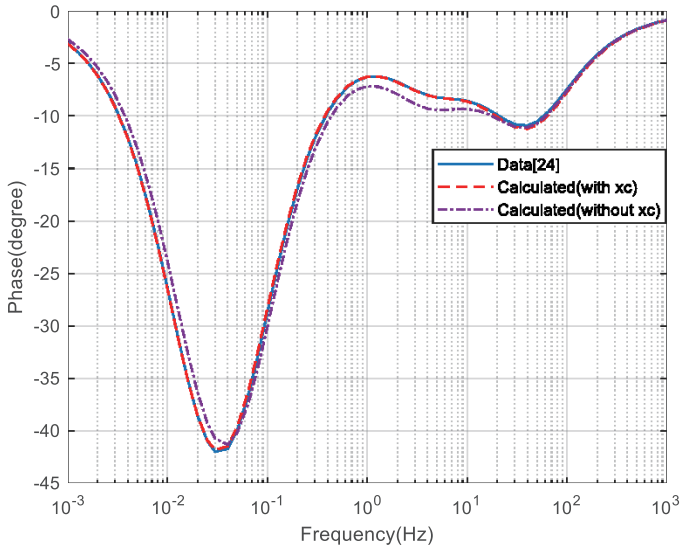

FIGURE 11. Operational inductance phase versus frequency (d-axis).

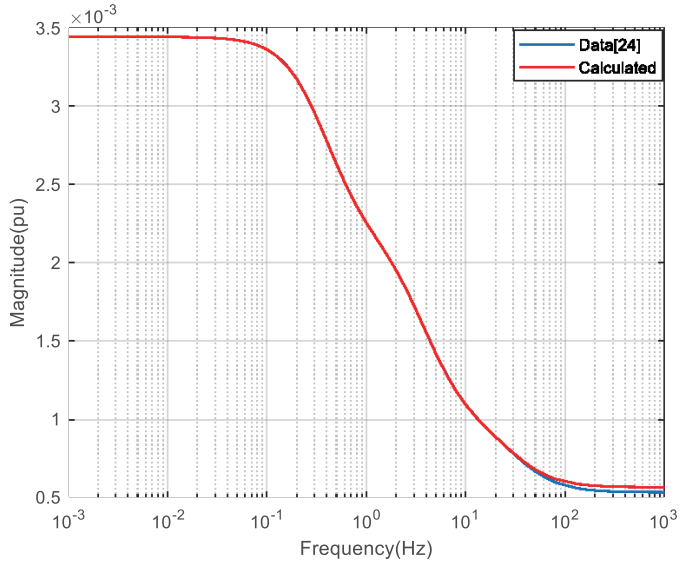

FIGURE 12. Operational inductance magnitude versus frequency (q-axis).

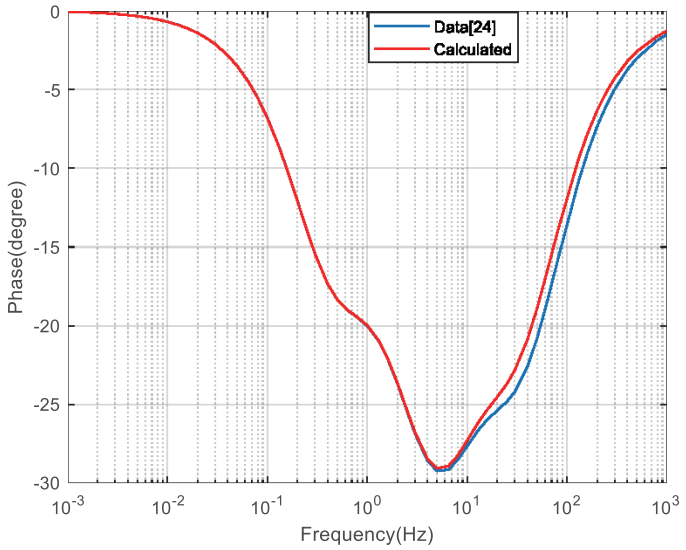

FIGURE 13. Operational inductance phase versus frequency (q-axis).

While this approach is straightforward and accessible, it is not without its challenges. There is a notable risk of the solution converging towards a local minimum, particularly influenced by the complexity of the model and the initial parameter values. The evolution of Canay model parameters across iterations is depicted in Figures 4 to 9, showing how they evolve as the iterations increases. It is interesting to note that the convergence of parameters L_f, R_f, R_k, and R_j occurs at the 8^{th} iteration, while parameters L_k and L_j converge at the 13^{th} iteration and 3^{th} iteration, respectively.

The parameters of the equivalent circuits of the third model with and without Canay reactance X_c are summarized in Table 2.

5.3. Results and Validation

To validate the results, the estimated parameters R_f, L_f, R_k, L_K, R_j, and L_j are introduced into the operational inductance transfer function in Equation (10).

While the time constants cited in the data are included in Equation (8), we compare the frequency responses of the two functions, by varying the frequency from 0.001 Hz to 1000 Hz.

Figures 10 and 11 show a perfect agreement between the Canay model and the data in terms of frequency responses. However, there is a clear difference in the frequency response of the conventional model and the data. The error on the magnitude varies from $-8.13.10^{-6}$ pu to $1.5.10^{-5}$ pu, while the phase error ranges from -0.4 degrees to 0.35 degrees.

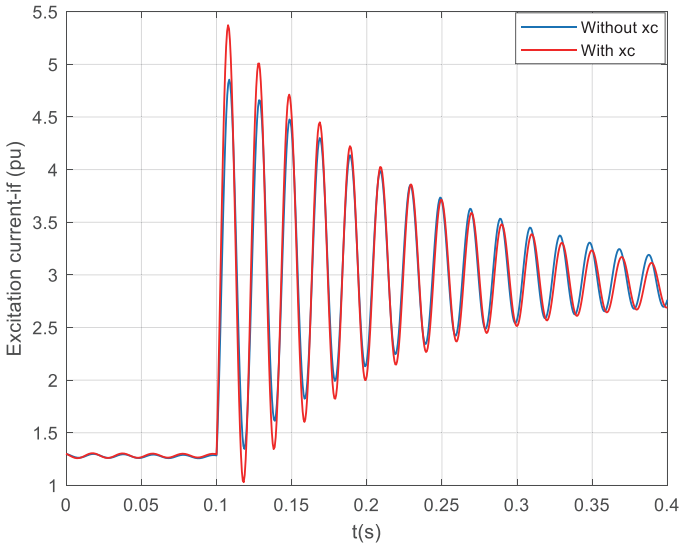

FIGURE 14. Variation of excitation current i_f during a three-phase short-circuit on load.

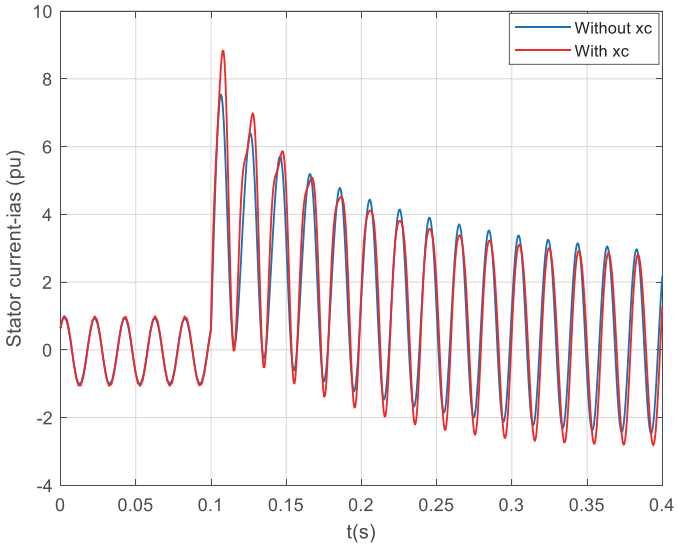

FIGURE 15. Variation of stator current i_{as} during a three-phase short-circuit on load.

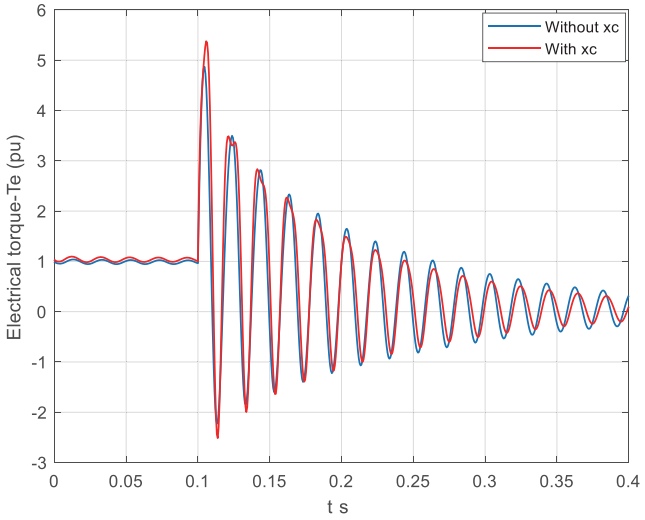

FIGURE 16. Variation of the electromagnetic torque T_e during a three-phase short circuit on load.

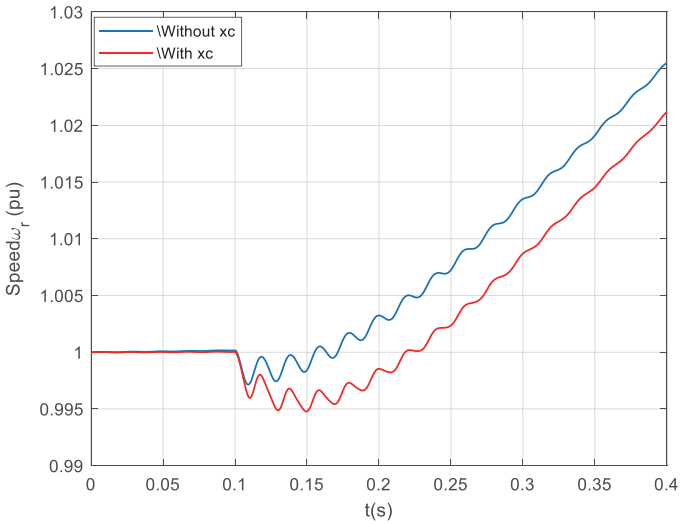

FIGURE 17. Variation of speed ω_r during a three-phase short circuit on load.

When examining the q axis in Figures 12 and 13, we can see a strong similarity between the model's frequency response and the data, with a minor phase difference for frequencies above 10 Hz.

6. EFFECT OF CANAY INDUCTANCE ON MACHINE DYNAMIC BEHAVIOUR

This part aims to carry out a comparative study of electromechanical quantities obtained using the traditional and the Canay models, for the dynamic system. To do this, we have implemented two applications: The first is to simulate a sudden three-phase short circuit, and the second is to study the dynamic stability.

6.1. Sudden Three-Phase Short Circuit

The choice of the short circuit time is arbitrary. However, in order to facilitate a precise analysis of the electromechanical quantities, we have chosen a relatively short circuit time. The simulation starts at the nominal point under load, with $V = 1$ pu, $\cos(\varphi) = 0.85$, and $\omega_r = 1$ pu. At time $t = 0.1$ s, a sudden three-phase short circuit is applied for a duration of 0.3 s. The simulation results are shown in Figures 14 to 19.

Figure 14 shows the variation of the excitation current as a function of time. The comparison of excitation short-circuit current curves reveals that the peaks of the Canay model are significantly higher than those of the conventional model.

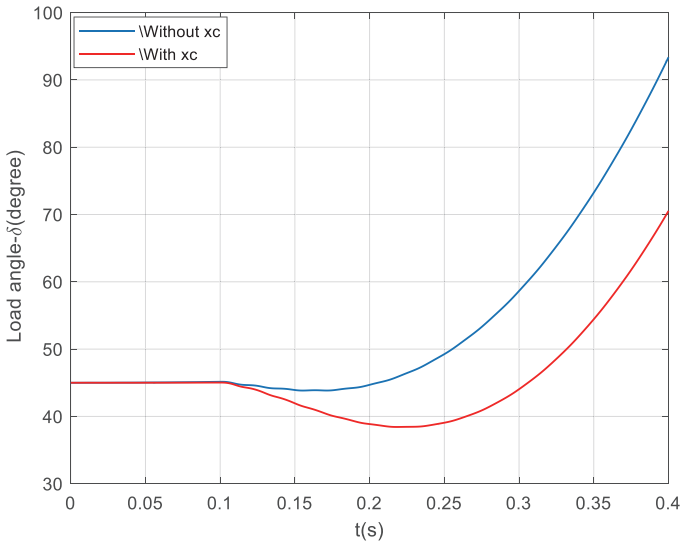

FIGURE 18. Variation of load angle δ during a three-phase short-circuit on load.

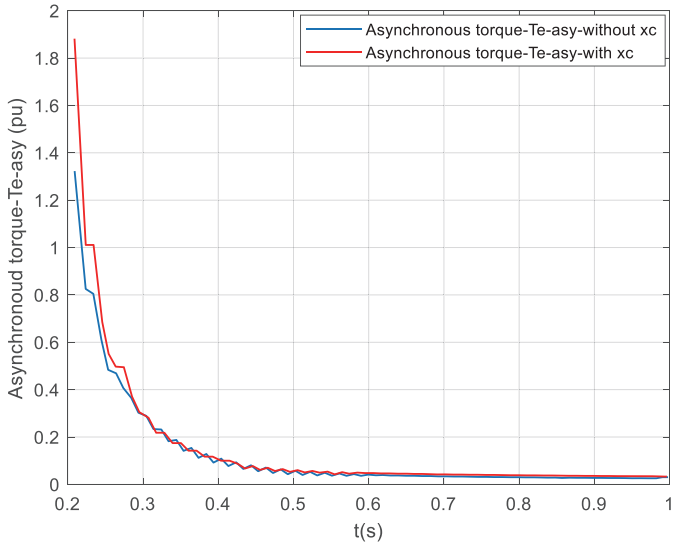

FIGURE 19. Variation of asynchronous braking torque versus time.

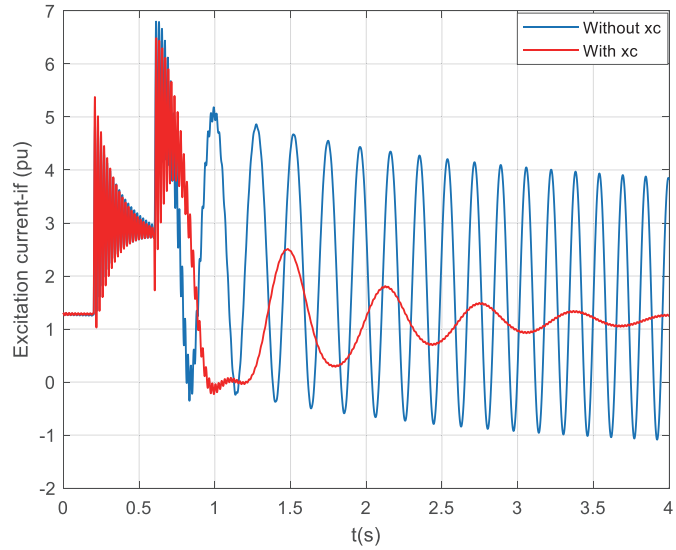

FIGURE 20. Variation of excitation current i_f when removing the three-phase short circuit on load.

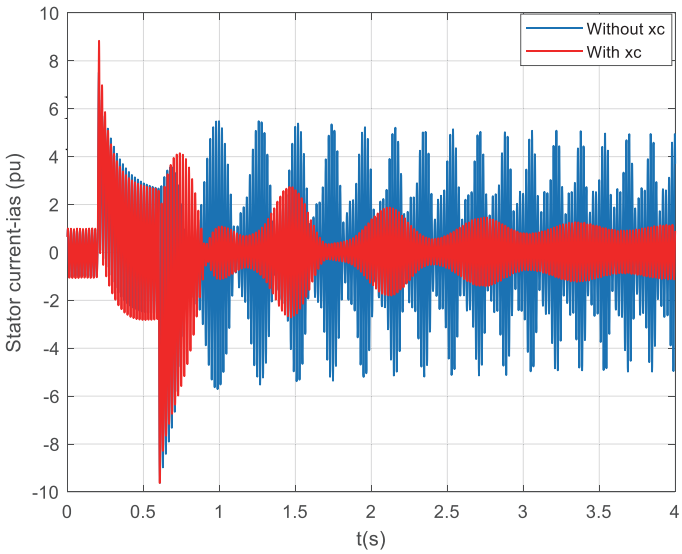

FIGURE 21. Variation of stator current i_{as} when removing the three-phase short circuit on load.

Figure 15 illustrates the variation of phase current i_a. A remarkable disparity between traditional and Canay models in the phase current is observed at the start of the short circuit.

Figures 16 to 19 present the temporal variations of the torque, speed, load angle, and asynchronous braking torque, respectively.

We notice a notable asymmetry in the electric torque, Figure 16. The average value of the oscillation indicates the asynchronous braking torque. It is worth noting that the asynchronous torque of the Canay model surpasses that of the conventional model, as depicted in Figure 19. This difference in torque becomes more pronounced as the load angle changes over time, as shown in Figure 18.

Initially, the asynchronous torque of the Canay model causes a small decrease in the load angle after 0.3 s, and it stabilizes at 68°. The back-swing process is represented inaccurately in the conventional model simulation, where the load angle increases more rapidly, reaching 93.5° after 0.3 s.

6.2. Dynamic Stability

The back-swing process exerts a significant influence on the stability of the generator [24], and thus it is of paramount im-

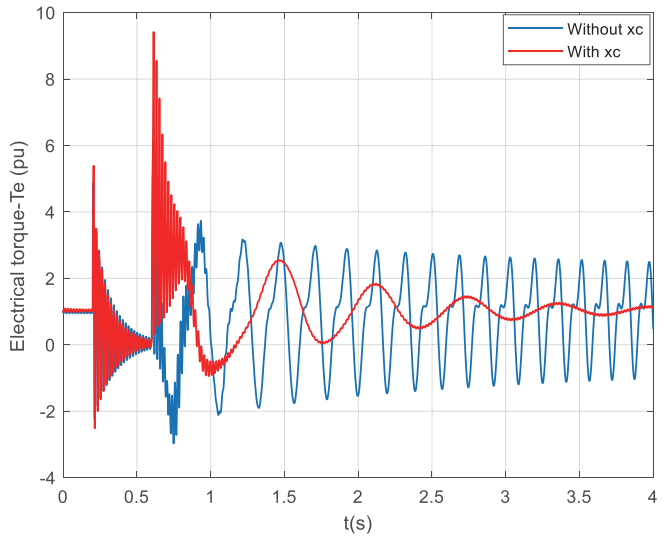

FIGURE 22. Variation of the electromagnetic torque T_e when removing the three-phase short circuit on load.

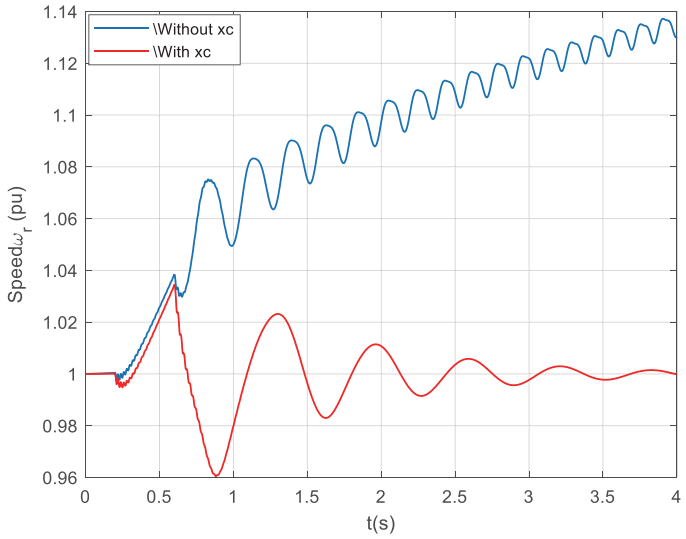

FIGURE 23. Variation of speed ω_r when removing the three-phase short circuit on load.

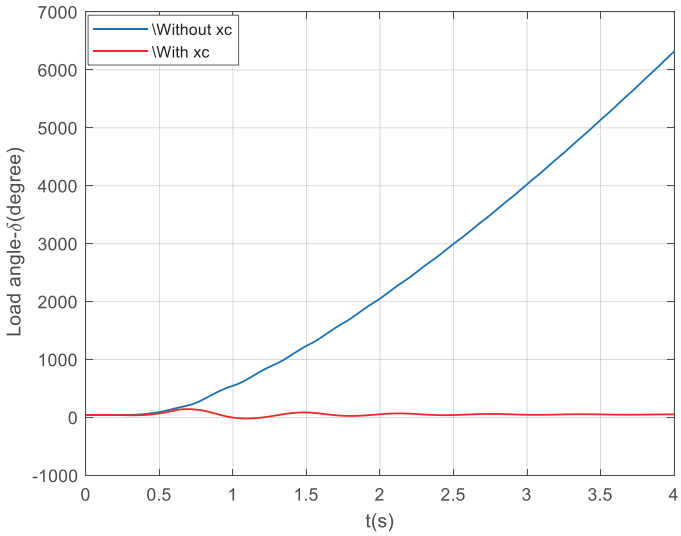

FIGURE 24. Variation of load angle δ when removing the three-phase short circuit on load.

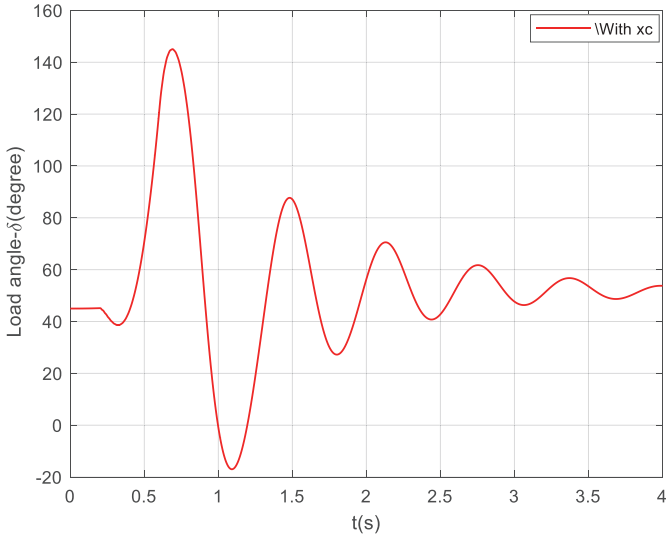

FIGURE 25. Variation of load angle δ when removing the three-phase short circuit on load.

portance to calculate it with the utmost accuracy. To illustrate this effect, the following application is performed. The simulation is applied from the nominal point with $V = 1$ pu, $\cos(\varphi) = 0.85$, $\omega_r = 1$ pu. The disturbance is a voltage drop of 0.4 s. From $t = 0.2$ s, the network voltage drops to 0 V and remains there for 0.40 s. After 0.60 s, the initial voltage value is restored. The simulation results are shown in Figures 20 to 25.

Canay model accurately reproduces the frequency characteristics of the machine. It is observed that the generator's loading angle increases to 118°and then returns to the nominal angle of 45°, showing the stability of the generator, Figure 25. In contrast, simulation using the conventional model indicates that the generator would lose synchronism, Figure 23.

This discrepancy arises from the conventional model's inability to accurately compute the braking asynchronous torque during a short circuit, as mentioned before. For Canay model, the field current, phase current, torque, and speed stabilize after a certain time $t = 4$ s.

7. CONCLUSION

This paper explores the potential of using an approach to estimate parameters for both conventional and Canay models. The results emphasize the importance of including Canay inductance to accurately reproduce the frequency characteristics of the direct axis operational inductance. In order to achieve accurate modeling and ensure faithful simulation of circuit quantities, the mutual leakage reactance between the windings of

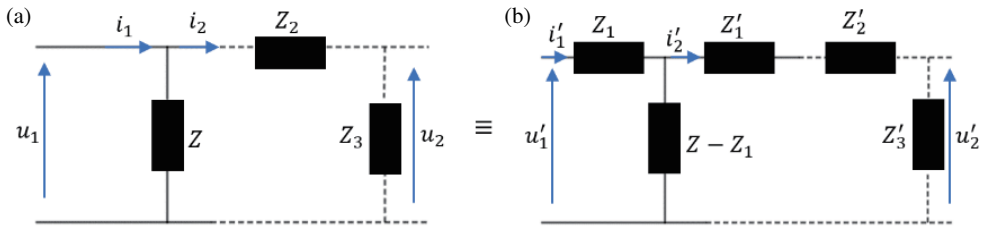

the field and damper was taken into account. Nevertheless, the Canay model was transformed to the traditional model with equal mutual reactances by a simple process to obtain the Canay reactance. Also, the study shows significant differences in quantities such as excitation current, electromagnetic torque, load angle, and speed between the Canay model and standard model during short-circuit testing under load.

In terms of dynamic stability, it was found that after a 0.42 s three-phase short-circuit and restoration of the rated voltage, the synchronous machine stabilizes at the synchronous speed according to the Canay model, while it loses the synchronism with the conventional model.

APPENDIX A. TRANSFORMATION

Circuits (a) and (b) are identical. Z'_1, Z'_2, i'_2, and u'_2 represent the transformed quantities. The voltage equation for the circuit (a) is:

$$u_1 = Z\left(i_1 - i_2\right) = Zi_1 + \left(Z - Z_1\right)\left(i_1 - \frac{Z}{Z - Z_1}i_2\right)$$

and results in a change:

$$\begin{cases} i'_2 = i_2/k_r \\ u'_2 = k_r i_2 \\ u'_2 = k_r i_2 \\ Z'_2 = k_r^2 Z_2, \ldots \\ k_r = \dfrac{Z - Z_1}{Z} \end{cases} \tag{A1}$$

This requires an impedance Z'_1 on the right side of circuit (b):

$$\begin{cases} u_2 = \left(i_1 - i_2\right) Z - Z_2 i_2 \\ u'_2 = \left(Z - Z_1\right)\left(i_1 - i'_2\right) - \left(Z'_1 + Z'_2\right) i'_2 \end{cases} \tag{A2}$$

While:

$$Z'_1 = -Z_1 k_r \tag{A3}$$

the impedance Z_1 can be chosen arbitrarily. If Z_1 has the same phase angle as Z, then the transformation constant k_r is a real quantity.

$$Z'_1 = -Z_1 \frac{Z - Z_1}{Z}$$

Application:

In order to demonstrate Equation (1), we proceeded as follows: $Z - Z_1 = \omega_s L_{md} = \omega_s\left(L_d - L_a\right) = X_d - X_a$, Figure 3 $Z = \omega_s L_{dc} = \omega_s(L_d - L_c) = X_d - X_c$, Figure 1.

Then: $Z_1 = \omega_s(L_{dc} - L_{md}) = X_a - X_c$, $k_r = \frac{Z - Z_1}{Z} = \frac{X_d - X_a}{X_d - X_c}$, $Z'_1 = -Z_1 k_r$. We obtain: $X_{rc} = -\left(X_a - X_c\right)\frac{X_d - X_a}{X_d - X_c} = -\left(X_a - X_c\right)\frac{X_{md}}{X_{md} + (X_a - X_c)}$

So, $-X_{rc} = \frac{X_{md}(X_a - X_c)}{X_{md} + (X_a - X_c)}$.

Finally: $\frac{1}{(X_c - X_a)} = \frac{1}{X_d - X_a} + \frac{1}{X_{rc}}$.

The diagrams of Figures (a) and (b) correspond to $L_d\left(s\right) - X_c$.

If we add the reactance X_c to the impedance $Z_1 = X_a - X_c$, we obtain the operational inductance $L_d\left(s\right)$ which corresponds to the diagram of Figure 3.

REFERENCES

[1] Park, R. H., "Definition of an ideal synchronous machine and formula for the armature flux linkage," *GE Review*, Vol. 31, No. 6, 332, 1928.

[2] Park, R. H. and B. L. Robertson, "The reactances of synchronous machines," *Transactions of the American Institute of Electrical Engineers*, Vol. 47, No. 2, 514–535, 1928.

[3] Park, R. H., "Two-reaction theory of synchronous machines generalized method of analysis-part I," *Transactions of the American Institute of Electrical Engineers*, Vol. 48, No. 3, 716–727, 1929.

[4] Park, R. H., "Two-reaction theory of synchronous machines-II," *Transactions of the American Institute of Electrical Engineers*, Vol. 52, No. 2, 352–354, 1933.

[5] Adkins, B. and R. G. Harley, "The General Equation of AC Machines," *The General Theory of Electrical Machines, Application to Practical Problems*, 58–97, Chapman and Hall London, UK, 1975.

[6] Robb, D. D. and P. C. Krause, "Dynamic simulation of generator faults using combined abc and 0dq variables," *IEEE Transactions on Power Apparatus and Systems*, Vol. 94, No. 6, 2084–2091, Nov. 1975.

[7] Ahmed-Zaid, S. and A. M. A. Oteafy, "A new interpretation of the steady-state two-reaction theory of a salient-pole synchronous machine," *IEEE Access*, Vol. 10, 128 187–128 194, 2022.

[8] Landgraf, T. G., E. P. T. Cari, and L. F. C. Alberto, "An analysis of structural and practical identifiability applied to a transient generator model," *Electric Power Systems Research*, Vol. 206, 107817, May 2022.

[9] Makram, E. B., V. O. Zambrano, R. G. Harley, and J. C. Balda, "Three-phase modeling for transient stability of large scale unbalanced distribution systems," *IEEE Transactions on Power Systems*, Vol. 4, No. 2, 487–493, 1989.

[10] Bai, X., T. Jiang, Z. Guo, Z. Yan, and Y. Ni, "A unified approach for processing unbalanced conditions in transient stability calculations," *IEEE Transactions on Power Systems*, Vol. 21, No. 1, 85–90, 2006.

[11] Elizondo, M. A., F. K. Tuffner, and K. P. Schneider, "Three-phase unbalanced transient dynamics and powerflow for modeling distribution systems with synchronous machines," *IEEE Transactions on Power Systems*, Vol. 31, No. 1, 105–115, 2016.

[12] Kadiman, S., O. Yuliani, and T. Handayani, "Teaching power system stabilizer and proportional-integral-derivative impacts on transient condition in synchronous generator," *Bulletin of Electrical Engineering and Informatics*, Vol. 10, No. 5, 2384–2395, Oct. 2021.

[13] Canay, I. M., "Causes of discrepancies on calculation of rotor quantities and exact equivalent diagrams of the synchronous machine," *IEEE Transactions on Power Apparatus and Systems*, Vol. PAS-88, No. 7, 1114–1120, Jul. 1969.

[14] Canay, I. M., "Determination of the model parameters of machines from the reactance operators x/sub d/(p), x/sub q/(p) (evaluation of standstill frequency response test)," *IEEE Transactions on Energy Conversion*, Vol. 8, No. 2, 272–279, Jun. 1993.

[15] Petrovic, D. S. and L. Pierrat, "An extended synchronous machine model and estimation of parameters by a step function response of blocked rotor," *Electric Machines and Power Systems*, Vol. 21, No. 5, 533–542, 1993.

[16] Sahoo, S. K., P. Rodriguez, and D. Savinovic, "Experimental investigation of different fault indicators for synchronous machine failure analysis," in *2015 IEEE International Electric Machines & Drives Conference (IEMDC)*, 1398–1404, Coeur d'Alene, ID, USA, 2015.

[17] Ni, S., G. Bauw, R. Romary, B. Cassoret, and J. L. Besnerais, "Damper winding for noise and vibration reduction of a permanent magnet synchronous machine," *Sensors*, Vol. 22, No. 7, 2738, Apr. 2022.

[18] Kadiman, S. and O. Yuliani, "Higher order model of synchronous generator," *International Journal of Power Electronics and Drive Systems (IJPEDS)*, Vol. 14, No. 3, 1442–1449, Sep. 2023.

[19] Tamura, J., R. Takahashi, T. Takazawa, Y. Tada, and A. Kurita, "Characteristics of canay inductance of synchronous machines and its effects on transient stability," *IEEJ Transactions on Industry Applications*, Vol. 124, No. 7, 706–715, 2004.

[20] Wunsch, B., S. Skibin, V. Forsstrom, and T. Christen, "Broadband modeling of magnetic components with saturation and hysteresis for circuit simulations of power converters," *IEEE Transactions on Magnetics*, Vol. 54, No. 11, 1–5, Nov. 2018.

[21] Chapariha, M., F. Therrien, J. Jatskevich, and H. W. Dommel, "Constant-parameter circuit-based models of synchronous machines," *IEEE Transactions on Energy Conversion*, Vol. 30, No. 2, 441–452, 2015.

[22] Chapariha, M., F. Therrien, J. Jatskevich, and H. W. Dommel, "Explicit formulations for constant-parameter voltage-behind-reactance interfacing of synchronous machine models," *IEEE Transactions on Energy Conversion*, Vol. 28, No. 4, 1053–1063, 2013.

[23] Hasni, M., "Identification paramétrique et structurale des machines synchrones par application de divers signaux d'excitation," Ph.D. dissertation, Ecole Nationale Polytechnique, Algiers, Algeria, 2007.

[24] Canay, I. M., "Physical significance of sub-subtransient quantities in dynamic behaviour of synchronous machines," in *IEE Proceedings B (Electric Power Applications)*, Vol. 135, No. 6, 334–340, Nov. 1988.

[25] Canay, I. M., "Modelling of alternating-current machines having multiple rotor circuits," *IEEE Transactions on Energy Conversion*, Vol. 8, No. 2, 280–296, Jun. 1993.

[26] Canay, I. M., "Determination of synchronous machine model parameters from the characteristic quantities applicable also to sub-subtransient data," *Electric Machines and Power Systems*, Vol. 9, No. 1, 33–47, 1984.

[27] Valverde, G., E. Kyriakides, G. T. Heydt, and V. Terzija, "Nonlinear estimation of synchronous machine parameters using operating data," *IEEE Transactions on Energy Conversion*, Vol. 26, No. 3, 831–839, Sep. 2011.